SUPPLEMENTARY INFORMATION

Rational design of a fluorescent NADPH derivative imaging constitutive nitric oxide synthases upon two-photon excitation.

Yun Li[*,||], Huan Wang[†,||], Bogdan Tarus[‡||], Miguel Romero Perez[§], Laurence Morellato[*], Etienne Henry[†], Vladimir Berka[¶], Ah-Lim Tsai[¶], Booma Ramassamy[*], Hamid Dhimane[*], Chantal Dessy[§], Patrick Tauc[†], Jean-Luc Boucher[*], Eric Deprez[†,**] and Anny Slama-Schwok[‡,**].

[*] Laboratoire de Chimie et Biochimie Pharmacologiques et Toxicologiques, CNRS UMR8601, Université Paris Descartes, Paris, France.

[†] Laboratoire de Biologie et Pharmacologie Appliquée (LBPA), CNRS UMR8113, ENS-Cachan, Cachan, France.

[‡] Laboratoire de Virologie et Immunologie Moléculaires, INRA UR892, Jouy en Josas, France.

[§] Pole of Pharmacology and Therapeutics, FATH5349, IREC, UCL Medical Sector, B-1200 Brussels, Belgium.

[¶] Division of Hematology, Department of Internal Medicine, University of Texas Health Science Center at Houston, Texas, USA.

[||] These co-first authors contributed equally to this work

[**] Eric Deprez and Anny Slama-Schwok contributed equally to the work.

Corresponding authors: Dr Anny Slama-Schwok Anny.Schwok@gmail.com,
And Dr Eric Deprez deprez@lbpa.ens-cachan.fr

Table of contents

SUPPLEMENTARY TABLE:

Table S1. Comparison of the interaction energies of bound NS1 and NT1 at the NADPH site of $nNOS_{red}$ as determined by molecular modelling.

Energy (kcal/mol)	NS1 in $nNOS_{red}$	NT1 in $nNOS_{red}$
Nucleotidic moiety:	- 458 ± 57	- 423 ± 26
Linker:	- 57 ± 6	- 38 ± 7
Chromophore:		
- Total	- 14 ± 7	- 26 ± 4
- van der Waals term	-39 ± 4	- 35 ± 3
- Electrostatic term	25 ± 5	9 ± 4
Total	- 529 ± 68	- 487 ± 25

SUPPLEMENTARY FIGURES:

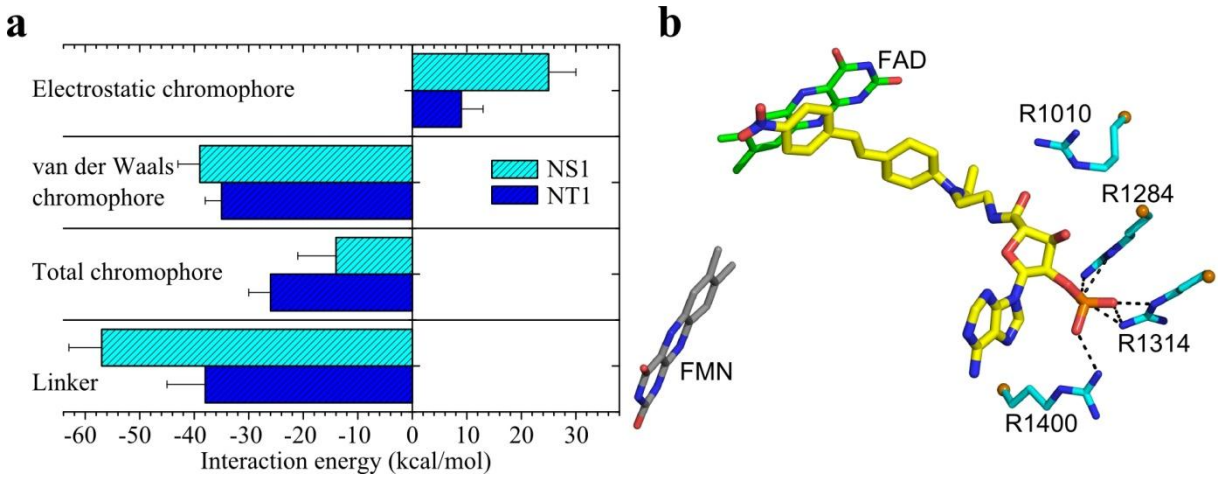

Fig. S1: (a) Effects of the linker and the chromophoric terminal group (NH_2 or NO_2) of NT1 or NS1 on the recognition of $nNOS_{red}$ at the NADPH site. Comparison of the interaction energies of the chromophore and linker parts of NS1 and NT1 with $nNOS_{red}$ (see also Table S1): the unfavorable electrostatic term is compensated by the van der Waals (VdW) interaction energies of the chromophore and the linker. **(b) NS1 binding in the NADPH site of nNOS reductase domain.** Overall binding of NS1 at the NADPH site by multiple H-bonds with conserved arginine residues of $nNOS_{red}$: the phosphate group of NS1 interacts with R1284, R1314 and R1400 and the carbonyl of the amide linker forms transient H-bond with R1010 while its chromophore terminal nitrophenyl group stacks on FAD.

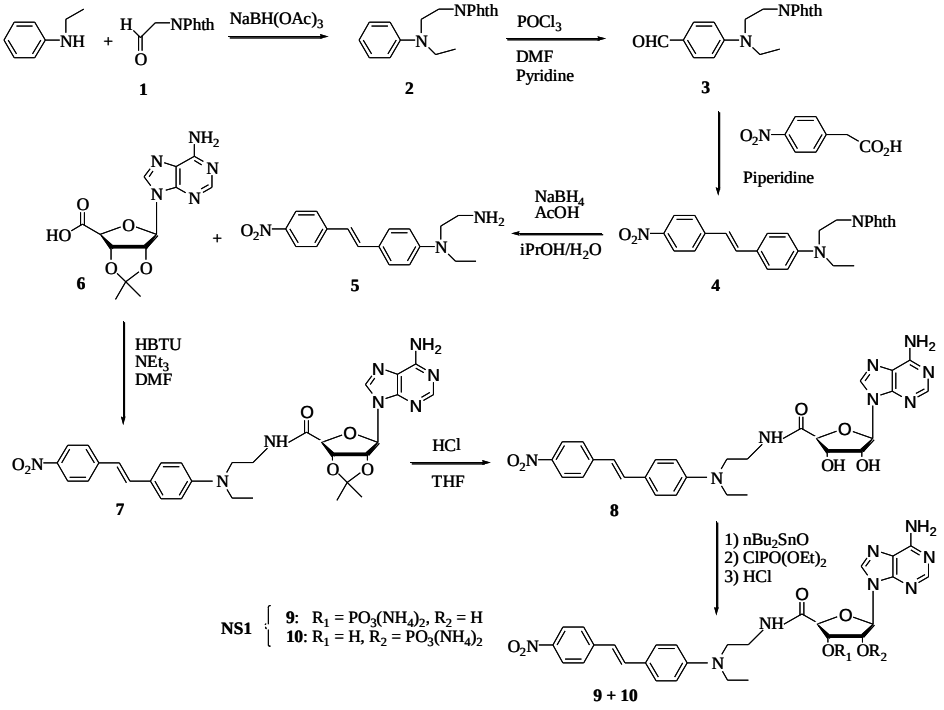

Fig. S2: Synthetic steps leading to NS1. The disubstituted aniline **2** was prepared by reductive amination of phthalimido-acetaldehyde **1** by *N*-ethylaniline in the presence of $NaBH(OAc)_3$. The substituted benzaldehyde **3** was prepared by a Vilsmeier's formylation of compound **2** under usual conditions ($POCl_3$ in DMF containing pyridine). The Knoevenagel's type condensation of 4-nitrophenyl-acetic acid with **3** led to the pure *E*-4-(4'-nitrostyryl)aniline derivative **4**. As the commonly used NH_2NH_2 method failed to deprotect the phthalimido group, it was removed using the $NaBH_4$-HOAc method giving the expected chromophore **5**. A peptide coupling reaction with HBTU in anhydrous DMF linked the chromophore **5** and the 2'-3'-*iso*-propylidene adenosine 5-carboxylic acid **6**. After HCl deprotection of the *iso*-propylidene moiety of compound **7**, diol **8** was phosphorylated at positions 2'- and 3'- by treatment with chlorodiethylphosphate in anhydrous CH_2Cl_2. Further acidic hydrolysis of the diethylphosphate afforded the expected compound NS1 as a mixture of two regioisomers **9** and **10** that bear the $P(O)(OH)_2$ group at positions 2'- and 3'- in a 40:60 ratio, respectively. See Supplementary Methods for more information.

These two isomers could be separated by analytical HPLC. Because these isomers can interconvert (1) and we estimated the Kd difference of the 2' over the 3' isomer not to exceed a factor 2-3, we did not attempt to set up conditions for a preparative separation of the 2' and 3' isomers (See Supplementary Methods for more information).

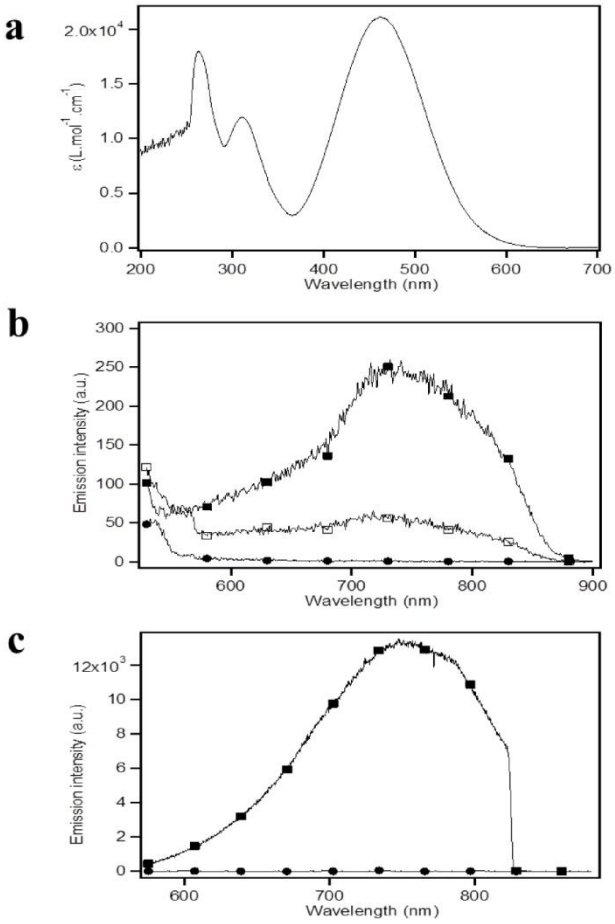

Fig. S3: Spectroscopic and fluorescence properties of NS1 in solution. (a) Absorption spectrum of NS1 in DMSO. **(b)** Fluorescence emission spectrum of NS1 (10 µM) upon one-photon excitation ($\lambda_{ex,1\text{-}PE}$ = 460 nm) in DMSO alone (black squares), in a DMSO : water mixture (67% : 33%, v:v) (white squares), or in 50 mM Tris buffer pH 7.5 containing 150 mM NaCl (black circles). **(c)** Fluorescence emission spectrum of NS1 (10 µM) upon two-photon excitation ($\lambda_{ex,2\text{-}PE}$ = 940 nm) in DMSO (black squares) or in 50 mM Tris buffer pH 7.5 containing 150 mM NaCl (black circles). The fluorescence quantum yield (Φ) and the two-photon cross-section (σ_2) of NS1 in DMSO were determined using rhodamine B as a reference and were found to be equal to 0.0045 and 65 GM at 940 nm, respectively. 1 Göppert-Mayer = 10^{-50} cm^4.s/photon.

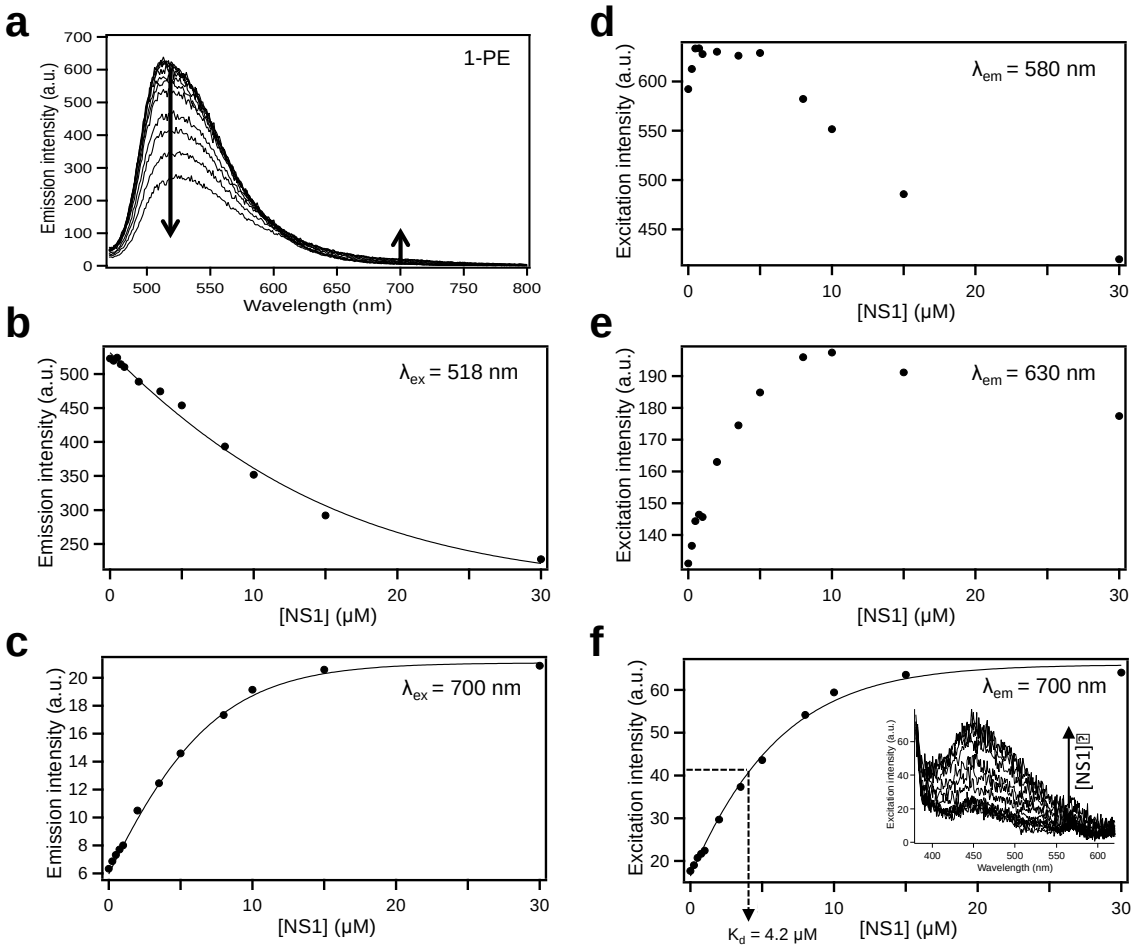

Fig. S4: Binding of NS1 to nNOS (5 μM) monitored by one-photon excitation fluorescence (1-PE). (a) Influence of NS1 on the fluorescence emission spectrum of nNOS ($\lambda_{ex,1\text{-}PE}$, 460 nm). The arrows indicate the decrease or increase in emission intensities at 518 or 700 nm, respectively, when increasing [NS1] (quantified in panels **b**-**c**). Panels **(d-f)**, the excitation intensity in the 430-490 nm range was plotted against [NS1]; λ_{em}: 580 **(d)**, 630 **(e)** or 700 nm **(f)** (**inset**: excitation spectra showing a continuous increase in the excitation intensity upon increasing [NS1]).

Using λ_{ex} = 460 nm, the emission intensity (518 nm) continuously decreased when increasing [NS1] (Fig. S4*a*). Concomitantly, the intensity increased on the red side of the emission spectrum (>610 nm), where the contribution of NS1 fluorescence is expected to be larger than the contribution of nNOS. Both changes in the intensity values reached a plateau upon increasing [NS1], indicating that NS1 actually bound to nNOS (Fig. S4*b*-*c*). As NS1 was not fluorescent in aqueous buffer, this indicated a recovery of NS1 fluorescence upon binding to nNOS. The decrease of the intensity (518 nm) is most likely due to a resonance energy transfer between FAD (donor) and NS1 (acceptor) that results from the significant overlap of FAD emission and NS1 absorption. Regarding the excitation intensity in the 430-490 nm region, using λ_{em} = 580 or 630 nm (Fig. S4*d*-*e*), a decreasing phase was observed when plotting the excitation intensity as a function of [NS1], consistent with the observed decrease in the emission intensity at 518 nm as mentioned above. This decreasing phase was less pronounced at 630 compared to 580 nm as the contribution of nNOS fluorescence relative to that of NS1 decreased by using a red-shifted λ_{em}. No decreasing phase was observed with λ_{em} = 700 nm, allowing quantitative titration of nNOS with NS1. A typical hyperbolic binding isotherm was obtained at this λ_{em} only (Fig. S4*f*; K_d = 4.2 ± 1.1 μM), but with a rather modest change in its intensity. The excitation maximum of NS1 bound to nNOS, 450 nm, was similar with NS1 absorption/excitation maximum in DMSO (Fig. S4*f*, inset).

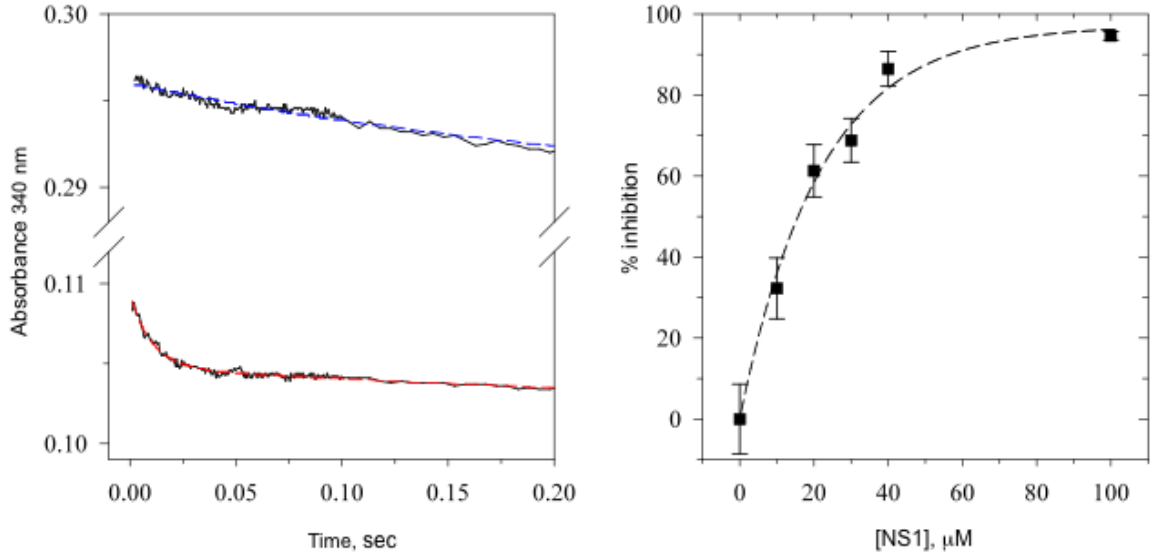

Fig. S5: Inhibition by NS1 of hydride transfer from NADPH to FAD in nNOS monitored by stopped-flow experiment. Left panel shows the raw absorbance changes at 340 nm after mixing of 25 μM NADPH with 5 μM nNOS (bottom trace) or 25μM NADPH with 100 μM NS1 and 5 μM nNOS (upper trace); the dashed lines represent bi-exponential fit of the data. Right panel shows that NS1 inhibited the fast phase in a dose-dependent saturable manner typical for competitive inhibition with NADPH. This fast phase is attributed to hydride transfer from NADPH to FAD. The slow phase remains unaffected by [NS1].

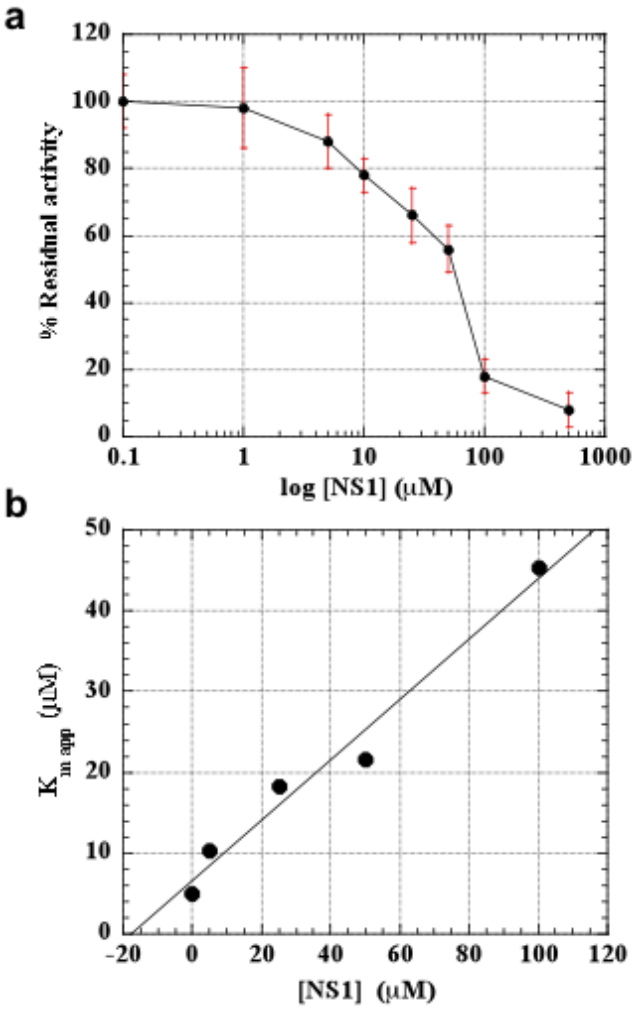

Fig. S6: Inhibition by NS1 of the formation of NO by nNOS: competition experiments between NADPH and NS1. Panel **(a)** shows the concentration-dependant inhibition of NO formation by NS1 in an assay performed in the presence of 100 µM NADPH. Maximal activity for nNOS was 78 ± 15 µM NO.min^{-1}.mM heme^{-1}. The IC_{50} value was found to be 65 µM. Using the Cheng-Prusoff (K_i = IC_{50}/(1+[NADPH]/K_d)), the K_i value was estimated to be 3.4 µM (assuming a K_m value of 5.5 µM). Panel **(b)** shows secondary plot of $K_{m\ app}$ as a function of NS1 concentration ($K_{m\ app}$ = K_m(1+[NS1]/K_i)). Intercept with the x-axis indicates a K_i value of 18 µM and the slope indicates a K_i value of 13 µM (assuming K_m = 5.5 µM). nNOS was incubated in 50 mM Hepes buffer at pH 7.4 containing 100 µM L-arginine, 100 µg/ml CaM, 1 mM $CaCl_2$, 100 U/ml SOD, 100 U/ml catalase and 8-10 µM oxyhemoglobin. Under identical conditions, the IC_{50} values for the endothelial NOS (maximal activity: 12 $\pm$ 5 µM NO.min^{-1}.mM heme^{-1}) and the inducible NOS (maximal activity: 150 $\pm$ 25 µM NO.min^{-1}.mM heme^{-1}) were 80 $\pm$ 15 µM and $\geq$ 200 µM, respectively.
The specific activities measured by hemoglobin and C^{14} arginine to citrulline conversion methods were in good agreement with each other and are as follows:
nNOS: 260 $\pm$ 50 nmole.min^{-1}.mg prot^{-1} (78 $\pm$ 15 s^{-1})
iNOS: 600 $\pm$ 100 nmole.min^{-1}.mg prot^{-1} (150 $\pm$ 25 s^{-1})
eNOS: 45 $\pm$ 22 nmole.min^{-1}.mg prot^{-1} (12 $\pm$ 5 s^{-1})

a

```
nNOS-rat   987 VHKKRVSAAR LLSRQNLQSP KFSRSTIFVR LHTNGNQELQ YQPGDHLGVF PGNHEDLVNA 1046
eNOS-rat   752 VHRRKMFQAT ILSVENLQSS KSTRATILVR LDTGSQEGLQ YQPGDHIGVC PPNRPGLVEA  811
iNOS-rat   724 IHAKNVFTMR LKSLQNLQSE KSSRTTLLVQ LTFEGSRGPS YLPGEHLGIF PGNQTALVQG  783
               :* :.:     : * :****  * :*:*:::*: *   ...  . * **:*:*:  * *:  **:.

nNOS-rat  1167 LSLLQPRYYS ISSSPDMYPD EVHLTVAIVS YHTRDGEGPV HHGVCSSWLN RIQADDVVPC 1226
eNOS-rat   931 LPLLQPRYYS VSSAPSAHPG EIHLTVAVLA YRTQDGLGPL HYGVCSTWMS QLKAGDPVPC  990
iNOS-rat   897 LPILKPRYYS ISSSQDHTPS EVHLTVAVVT YRTRDGQGPL HHGVCSTWIN NLKPEDPVPC  956
               *.:*:***** :**: .  *. *:*****:::: *:*:** **: *:****:*:. .::. * ***

nNOS-rat  1227 FVRGAPSFHL PRNPQVPCIL VGPGTGIAPF RSFWQQRQFD IQHKGMNPCP MVLVFGCRQS 1286
eNOS-rat   991 FIRGAPSFRL PPDPNLPCIL VGPGTGIAPF RGFWQDRLHD IEIKGLQPAP MTLVFGCRCS 1050
iNOS-rat   957 FVRSVSGFQL PEDPSQPCIL IGPGTGIAPF RSFWQQRLHD SQHRGLKGGR MTLVFGCRHP 1016
               *:*....*:* * :*. **** :********* *.***:* .*  : :*::    *.******  .

nNOS-rat  1287 KIDHIYREET LQAKNKGVFR ELYTAYSREP DRPKKYVQDV LQEQLAESVY RALKEQGGHI 1346
eNOS-rat  1051 QLDHLYRDEV LDAQQRGVFG QVLTAFSRDP GSPKTYVQDL LRTELAAEVH RVLCLEQGHM 1110
iNOS-rat  1017 EEDHLYQEEM QEMVRKGVLF QVHTGYSRLP GKPKVYVQDI LQKELADEVF SVLHGEQGHL 1076
               : **:*::*   :  .:**:  :: *.:** * . ** ****: *: :** .*.  .*  : **:

nNOS-rat  1347 YVCGDVTMAA DVLKAIQRIM TQQGKLSEED AGVFISRLRD DNRYHEDIFG VTLRTYEVTN 1406
eNOS-rat  1111 FVCGDVTMAT SVLQTVQRIL ATEGSMELDE AGDVIGVLRD QQRYHEDIFG LTLRTQEVTS 1170
iNOS-rat  1077 YVCGDVRMAR DVATTLKKLV AAKLNLSEEQ VEDYFFQLKS QKRYHEDIFG AVFSYGAKKG 1136
               :****** **  .*  :::::: : : .:. :: .   :  *:. ::********** .:    ..
```

Hydrophobic patch
Conserved residues at 5 Å from the chromophore
Phosphate binding
Variable residues at 5 Å from the chromophore
Most important variable residues

b

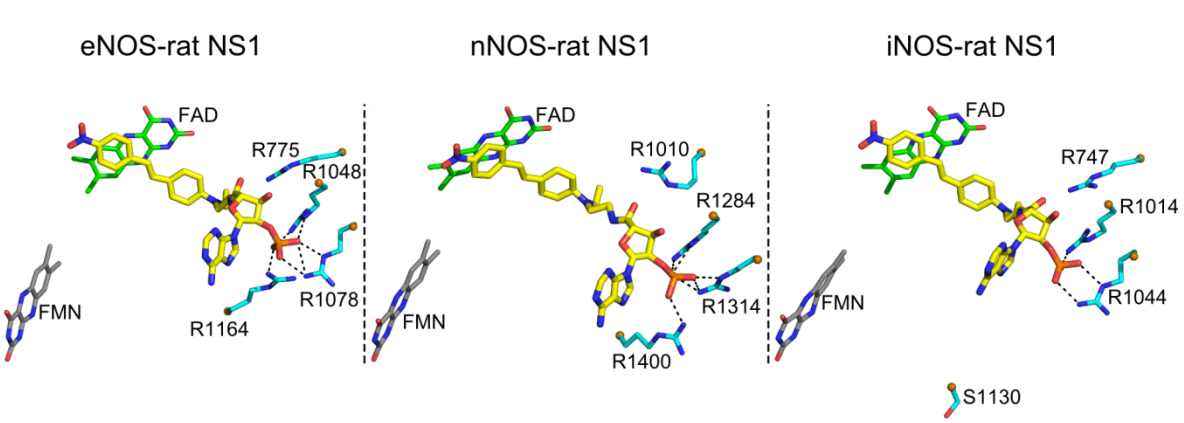

Fig. S7: (a) Alignment of NOS reductase domains and identification of residues within 5 Å to NS1. (b) Comparison of NS1 binding in the NADPH site of eNOS, nNOS and iNOS reductase domains. The 3D-structures of eNOS (left) and iNOS (right) were generated by homology modeling as described (2) (see also supplementary methods). Docking of NS1 in iNOS differed from that in nNOS (or eNOS) by the replacement of R1400 (or R1164) by S1130; thus, the electrostatic interaction between NS1 phosphate and R1400 (or R1164) found in nNOS (or eNOS) lacks in iNOS.

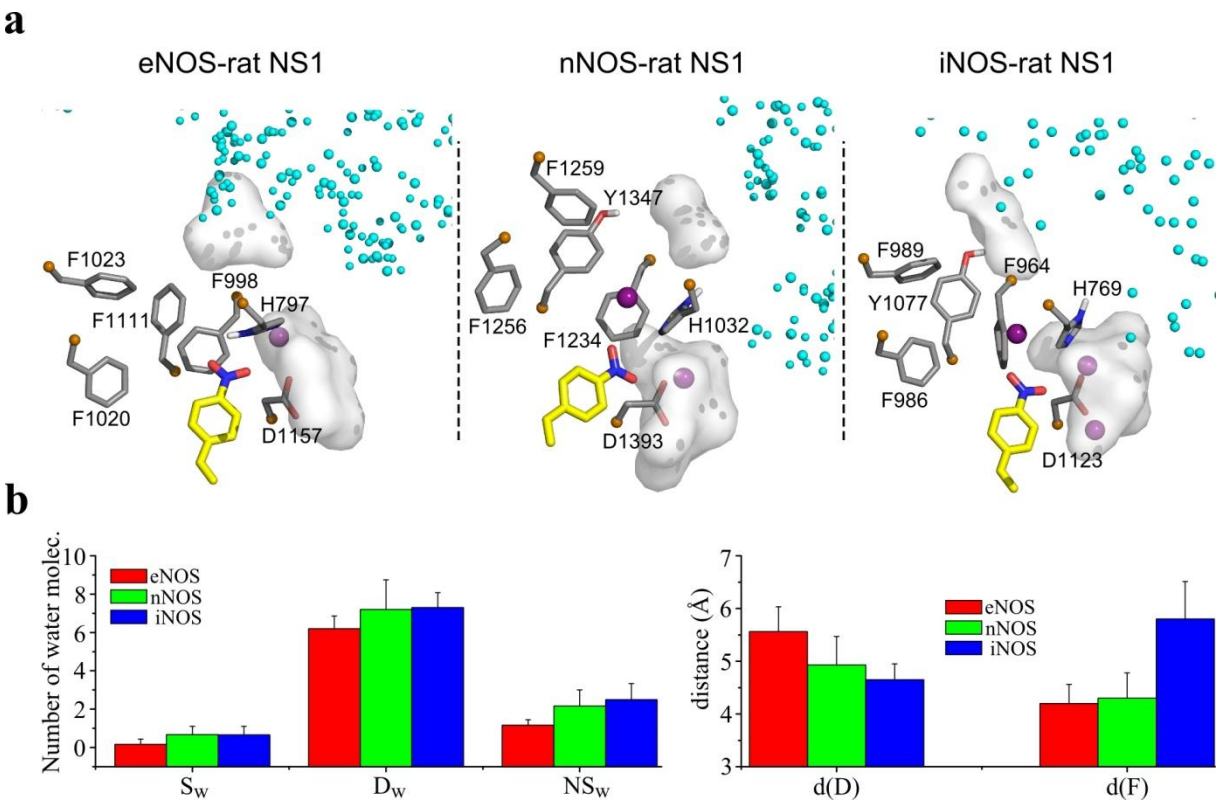

Fig. S8: (a) Structural insight on the solvation and hydrophobic patch in NS1 binding site zoomed at NS1 nitrophenyl terminal in three NOS isoforms. Solvation of D1393 and Y1347 is highlighted by white surfaces; water at 3.5 Å from the nitro group of NS1 is shown by large purple spheres while the water at 3.5Å from the interface between NOS monomers is depicted by small cyan spheres. **(b) Comparison of selected distances and solvation around the NO_2 terminal of NS1 in the three NOS isoforms as defined in the text below**.

To get quantitative estimates on the differences in solvation around NS1 between the three isoforms, we characterized the following:

- **NS_w**, the number of water at a distance of 3.5 Å to the nitro group of NS1, related to the residence of water molecules around NS1 chromophore; panels (a) and (b) show that NS_w is lowest in eNOS compared to the water found in nNOS and iNOS.
- **D_w**, the number of water molecules solvating D1393; D_w is within the error similar in eNOS, nNOS or iNOS, accounting for 6 to 8 water molecules.
- **S_w**, the solvation of Ser1176 by "catalytic" water and/or by His1032. The lowest number of water molecules around S940 is found in eNOS while S940 is closest to H797 in eNOS compared to both nNOS and iNOS. Previous point mutation studies have shown that the water molecule ("catalytic" water) around Ser1176 (nNOS) has a key role in the proton transfer as part of the hydride transfer step (in a general acid/base in the protonation / deprotonation of the N1 atom of the flavin that is necessary during catalysis (3-5).
- **d_D**, the minimum distance between side-chain heavy atoms of D1393, D1157 or D1123 (n/e/iNOS) to the N atom of nitro group, d_D, is largest in eNOS and decreases in nNOS and iNOS (panel (a)).
- **d_F**, the minimum distance between side-chain heavy atoms distance of F1234, F998 or F964 (n/e/iNOS) to the the N atom nitro group, dF is largest in iNOS compared to eNOS and nNOS.

Additional comment to Fig. S8:

Therefore, the NO_2 group in iNOS probes a more solvated environment. In contrast, the NO_2 group of NS1 in eNOS is located in the relatively more hydrophobic environment than in the two other NOS isoforms, characterized by the lowest distance to the conserved F998 and closest to the hydrophobic patch as compared to nNOS and iNOS (see also Fig. 3). Altogether, NS1 probes a more hydrophobic environment in eNOS by a combination of light sequences changes, resulting in stronger hydrophobic interactions and less solvation. This effect is gradual from eNOS, through nNOS to iNOS. These hypotheses perfectly explain the decrease of fluorescent yield of NS1 from eNOS to iNOS, (NS1 in eNOS being the highest, Fig. 3) by local environment effects. This is in agreement with the previously reported decrease in the nitroaminostilbene fluorescence yield in DMSO as compared to CH_2Cl_2 (6). We cannot exclude that global effects at larger distance from NS1 arising from water at the protein – solvent interface could also contribute to explain the experimental findings. We did not observe a distortion of NS1 chromophore from planarity which is expected to affect the overall dipolar moment and the fluorescence yield by some character of "twisted" charge transfer state. It is likely that twisting around the double bond is impeded by steric effects in the NADPH binding site.

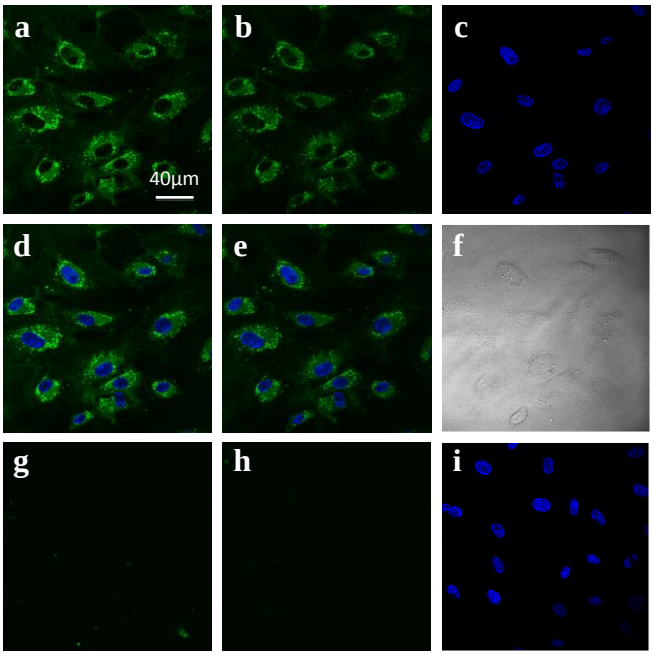

Fig. S9: Imaging of living HUVECs using one- or two-photon excitation of NS1. HUVECs were treated with NS1 (5 µM) and further observed under either one-photon excitation (confocal microscopy; excitation, 488 nm) **(a)** or two-photon excitation (multiphoton microscopy; excitation, 840 nm) **(b)**. Emission setting was 520-680 nm. Panel **(c)** shows the nucleus staining of NS1-treated HUVECs by Hoechst 33342 (two-photon excitation, 740 nm; emission setting: 410-510 nm). Panels **(d)** and **(e)**: corresponding merges for one- and two-photon images, respectively. Panel **(f)**, DIC transmission image. Control cells (not treated with NS1) were observed under one-photon **(g)** or two-photon **(h)** excitation using the same settings as described for panels **(a)** and **(b)**, respectively. Panel **(i)** shows the nucleus staining of control HUVECs (not treated with NS1) by Hoechst 33342 (two-photon excitation, 740 nm).

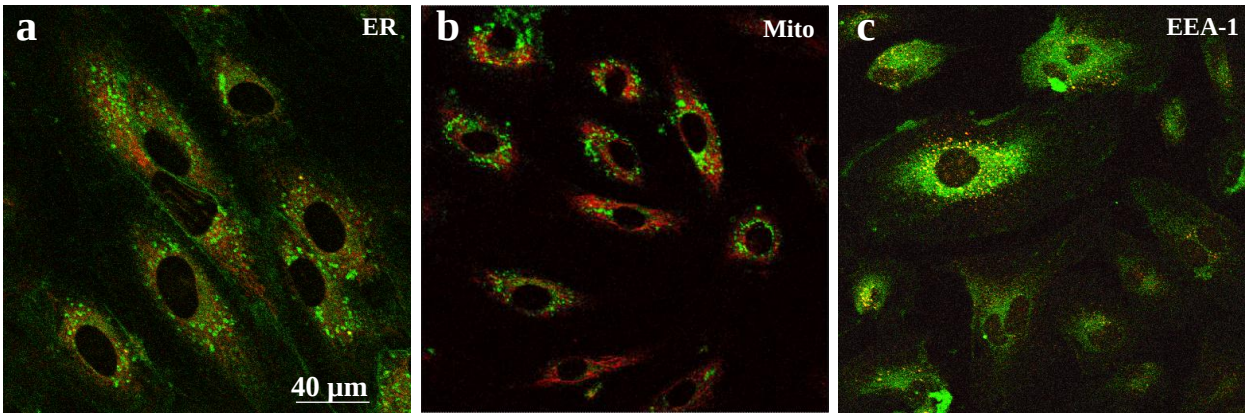

Fig. S10: Co-localization imaging of NS1 and Endoplasmic Reticulum (ER), Mitochondria or Early Endosome (EEA1). (a) Merged image of NS1 and ER. **(b)** Merged image of NS1 and mitochondria. Living HUVECs were treated with NS1 (5 µM) and ER tracker (ER-TrackerTM Red dye; 100 nM) or MitoTracker (MitoTracker® Deep Red FM; 50 nM) for 30 min and further observed under confocal microscopy. **(c)** Merged image of NS1 and EEA1. Living HUVECs were treated with NS1 (10 µM) for 60 min prior to fixation and immuno-staining of EEA1, and further observed under confocal microcopy. Primary and secondary antibodies for immuno-staining were rabbit polyclonal to EEA1-Early Endosome Marker and Alexa Fluor® 594 donkey anti-rabbit IgG (H+L), respectively. Excitation and emission settings: NS1 (exc. 488 nm; em. 520-680 nm), ER (exc. 543 nm; em. 590-670 nm), mitochondria (exc. 633 nm; em. 650-700 nm), EEA1 (exc. 543 nm; em. 590-700 nm).

SUPPLEMENTARY METHODS:

Molecular modelling. The MD simulations of the nNOS-NS1 and nNOS-NT1 complexes and eNOS-NS1, iNOS-NS1 complexes (the reductase domains of eNOS and iNOS were generated by homology modelling, see below) were carried out using the program NAMD (7) with the CHARMM27 force field (8). The solvent was treated explicitly using the TIP3P model for water molecules (9). The system formed by nNOS (or eNOS rat or iNOS rat) dimeric enzyme, FAD, FMN and NS1 (or NT1) was centred in a cubic cell of pre-equilibrated water molecules. The electrostatic interactions were calculated with no truncation, using the particle mesh Ewald summation algorithm (10). The system was made electrostatically neutral by adding sodium cations at coordinates of minimum electrostatic energy. The ion concentration of the system was set to 0.15 M by adding randomly sodium and chloride ions. The van der Waals interactions were smoothly shifted to zero between 10.0 Å and 12.0 Å. The list of the non-bonded interactions was truncated at 13.5 Å. The energy of the system was minimized during 5000 steps using the conjugate gradient energy minimization algorithm while the solute atoms were harmonically restraint to their initial positions with a force constant of 50.0 kcal/mol/Å^2. The system was heated linearly to 300 K over 60 ps. The lengths of the bonds containing hydrogen atoms were fixed with the SHAKE algorithm (11) and the equations of motion were iterated using a time step of 2 fs in the velocity Verlet integrator. Molecular dynamics simulation was further used to equilibrate the system and for production run. During the equilibration phase, the restrains applied on the solute atoms were gradually reduced from 5.0 kcal/mol/Å^2 to zero. The pressure and temperature were restrained to 1 atm and 300 K, respectively. Each system was simulated for 10 ns.

Homology modelling of eNOS-rat and iNOS-rat reductase domains. Homology modeling was performed using the x-ray structure of the neuronal NOS (nNOS-rat, PDB-ID: 1TLL) as template. The structure of the eNOS-rat was solved by homology modeling as reported previously (1).The iNOS-rat sequence was aligned on the nNOS-rat sequence using the ClustalX 2.1 program (11). Based on the sequence alignment and the coordinates of the monomeric form of the nNOS-rat (PDB id 1TLL), a Swiss-PdbViewer (12) project was made and submitted to the homology modeling website Swiss-Model Workspace (13). The sequence alignment (shown in Fig S7) revealed for the eNOS-rat 374 identical (56.3 %) and 139 similar (20.9 %) positions, accounting for a 77.3 % total homology. For the iNOS-rat there were found 305 identical (45.9%) and 139 similar (20.9%) positions, accounting for a 66.9 % total homology and a QMEAN score (14) of 0.659.

Chemistry, General. All reagents and solvents were from Sigma-Aldrich (Saint-Quentin-Fallavier, France) and were of the highest purity commercially available. High-purity argon (99.9995%) was obtained from Air Products. Phthalimidoacetaldehyde diethyl acetal (**1**) and 2',3'-*O*-isopropylidene adenosine carboxylic acid (**6**) were prepared from aminoacetaldehyde diethyl acetal and 2',3'-*O*-isopropylidene adenosine, respectively, according to known procedures (12, 13).

TLC was performed on pre-coated plates of Silica Gel 60F-254 (Merck, Lyon, France); compounds were detected by UV light. ^{1}H and ^{13}C NMR spectra were recorded with a Bruker (Wissembourg, France) Biospin Avance II 250 MHz spectrometer, and chemical shifts refer to an internal standard of Me_4Si. Mass spectra were recorded by electrospray ionization (ESI) in both positive (ESI^+) and negative (ESI^-) ionization detection modes with a LCQ Advantage ion trap mass spectrometer (Thermo, Les Ulis, France). Elemental analyses were performed at ICSN (Gif sur Yvette, France) and high-resolution mass spectra (HRMS) were obtained by ESI in time-of-flight (TOF) detection mode on a LCT (Waters-Micromass, Guyancourt, France) spectrometer at ICSN (Gif sur Yvette, France).

Synthesis of NS1: The NADPH analogue NS1 was prepared as described in Fig. S2.

N-[2-(N-Ethylanilino)ethyl]phthalimide (**2**): $NaBH(OAc)_3$ (3.05 g, 14.4 mmol) was added to a solution of *N*-ethylaniline (1.16 g ; 9.6 mmol) and **1** (2.72 g, 14.4 mmol) in CH_2Cl_2 (28 mL). After 24 h at 20 °C, CH_2Cl_2 was added and the organic phase was washed with H_2O, dried ($MgSO_4$) and evaporated. The crude product was purified by chromatography over silica gel (80:20 CH_2Cl_2–cyclohexane) to afford **2** as a yellow solid (2.71 g, 96 %). ^{1}H NMR (250 MHz, $CDCl_3$): δ 7.85 (m, 2H), 7.71 (m, 2H), 7.24 (t, J = 7.8 Hz, 2H), 6.86 (d, J = 7.8 Hz, 2H), 6.67 (t, J = 7.8 Hz, 1H), 3.91 (dd, J = 6.5, 8.1 Hz, 2H), 3.58 (dd, J = 6.5, 8.1 Hz, 2H), 3.46 (q, J = 6.9 Hz, 2H), 1.22 (t, J = 7.0 Hz, 3H). ^{13}C NMR (63 MHz, $CDCl_3$): δ 168.0 (C), 147.2 (C), 133.7 (CH), 131.8 (C), 129.2 (CH),

123.0 (CH), 116.0 (CH), 111.9 (CH), 47.8 (CH_2), 44.6 (CH_2), 35.0 (CH_2), 12.2 (CH_3). MS: m/z = 295 (MH^+). Anal. calcd for $C_{18}H_{18}N_2O_2$ (294.14), C 73.45, H 6.16, N 9.52. Found C 73.33, H 6.17, N 9.62.

N-[2-(N-Ethyl-4-formyl-anilino)ethyl]phthalimide (**3**) $POCl_3$ (5.24 mL) was added dropwise to a solution of **2** (2.71 g, 9.2 mmol) in anhydrous pyridine (4.50 mL) and DMF (55 mL), at 0 °C under an argon atmosphere. After 24 h at 20 °C, ice (~ 600 g) was added and stirred for 30 min. The precipitate was filtered, washed and dissolved with CH_2Cl_2. The organic phase was separated from H_2O, dried ($MgSO_4$) and evaporated. The crude product was filtered over silica gel (Et_2O) to afford **3** as a pale yellow solid after evaporation of the solvent (2.84 g, 96 %). ^{1}H NMR (250 MHz, $CDCl_3$): δ 9.67 (s, 1H), 7.82 (m, 2H), 7.69 (m, 4H), 6.81 (d, J = 8.9 Hz, 2H), 3.89 (dd, J = 6.6, 7.3 Hz, 2H), 3.63 (dd, J = 6.6, 7.3 Hz, 2H), 3.50 (q, J = 7.3 Hz, 2H), 1.21 (t, J = 7.3 Hz, 3H). ^{13}C NMR (63 MHz, $CDCl_3$): δ 189.9 (CH), 168.0 (C), 152.0 (C), 134.0 (CH), 132.1 (CH), 131.6 (C), 125.2 (C), 123.2 (CH), 111.8 (CH), 47.6 (CH_2), 44.9 (CH_2), 34.6 (CH_2), 12.1 (CH_3). MS: m/z = 323 (MH^+). Anal. calcd for $C_{19}H_{18}N_2O_3$ (322.13), C 70.79, H 5.63, N 8.69. Found C 70.28, H 5.62, N 8.62.

N-{2-[N-Ethyl-(4-nitro-phenyl)-vinyl-anilino]ethyl}phthalimide (**4**): A solution of 4-nitrophenyl acetic acid (1.55 g, 8.6 mmol) and piperidine (655 mg, 7.7 mmol) in CH_2Cl_2 (~ 10 mL) was stirred at 20 °C for 10 min. Aldehyde **3** (2.48 g, 7.7 mmol) was then added to the mixture. After 10 min at 20 °C, CH_2Cl_2 was evaporated, and the reaction was heated at 100 °C under vacuum (15 mm Hg) for 3 h, then at 150 °C / 15 mm Hg for 3 h. The crude product was purified by chromatography over silica gel (80:20 CH_2Cl_2–cyclohexane) to afford **4** as a red solid (2.21 g, 65 %). ^{1}H NMR (500 MHz, $CDCl_3$): δ 8.16 (d, J = 8.9 Hz, 2H), 7.83 (m, 2H), 7.70 (m, 2H), 7.53 (d, J = 8.9 Hz, 2H), 7.40 (d, J = 8.8 Hz, 2H), 7.14 (d, J = 16.2 Hz, 1H), 6.87 (d, J = 16.2 Hz, 1H), 6.80 (d, J = 8.9 Hz, 2H), 3.88 (dd, J = 6.7, 8.1 Hz, 2H), 3.58 (dd, J = 6.7, 8.1 Hz, 2H), 3.46 (q, J = 7.0 Hz, 2H), 1.20 (t, J = 7.0 Hz, 3H). ^{13}C NMR (63 MHz, $CDCl_3$): δ 168.3 (C), 148.0 (C), 145.9 (C), 145.0 (C), 134.1 (CH), 133.5 (CH), 132.0 (C), 128.7 (CH), 126.1 (CH), 124.5 (C), 124.1 (CH), 123.3 (CH), 121.7 (CH), 112.1 (CH), 48.0 (CH_2), 45.1 (CH_2), 35.1 (CH_2), 12.4 (CH_3). MS: m/z = 442 (MH^+). Anal. calcd for $C_{26}H_{23}N_3O_4$ (441.17), C 70.73, H 5.25, N 9.52. Found C 70.19, H 5.13, N 9.53.

2-[N-Ethyl-(4-nitro-phenyl)-vinyl-anilino]ethylamine (**5**): $NaBH_4$ (806 mg, 21.5 mmol) was added to a suspension of **4** (1.88 g, 4.3 mmol) in a mixture of 2-propanol / water (6 / 1, 120 mL). After 1 h at 60 °C, acetic acid (8 mL) was added at 20 °C and the reaction was kept at 80 °C for 48 h. 2-Propanol was evaporated and the precipitate was filtered. The crude product was purified by chromatography over silica gel (MeOH:CH_2Cl_2:NH_4OH = 3:97:0.25) to afford **6** as a red solid (1.02 g, 77 %). ^{1}H NMR (250 MHz, DMSO-d_6): δ 8.17 (d, J = 8.9 Hz, 2H), 7.75 (d, J = 8.9 Hz, 2H), 7.49 (d, J = 8.9 Hz, 2H), 7.41 (d, J = 16.4 Hz, 1H), 7.10 (d, J = 16.4 Hz, 1H), 6.76 (d, J = 8.9 Hz, 2H), 3.42 (m, 4H), 2.83 (t, J = 6.6 Hz, 2H), 1.09 (t, J = 7.0 Hz, 3H). ^{13}C NMR (63 MHz, DMSO-d_6): δ 148.1 (C), 145.2 (C), 145.1 (C), 133.9 (CH), 128.7 (CH), 126.3 (CH), 124.0 (CH), 123.6 (C), 120.9 (CH), 111.6 (CH), 49.8 (CH_2), 44.4 (CH_2), 37.8 (CH_2), 12.0 (CH_3). HRMS (ESI) calcd for $C_{18}H_{22}N_3O_2$ (MH^+) *m/z* 312.1712, found 312.1701.

*Compound **7***: Et_3N (0.8 mL) and HBTU (2.18 g, 5.7 mmol) were added to a solution of **5** (1.19 g, 3.8 mmol) and 2',3'-*O*-isopropylidene adenosine carboxylic acid **6** (1.23 g, 3.8 mmol) in anhydrous DMF (130 mL). After 48 h at 20 °C under an argon atmosphere, DMF was evaporated and the usual work-up with EtOAc / H_2O gave the crude product which was purified by chromatography over silica gel (60:40 EtOAc–CH_2Cl_2) to afford **7** as a red solid (1.64 g, 70 %). ^{1}H NMR (250 MHz, DMSO-d_6): δ 8.29 (s, 1H), 8.17 (d, J = 8.8 Hz, 2H), 8.11 (s,1H), 7.75 (d, J = 8.8 Hz, 2H), 7.72 (s, 1H, D_2O exchangable), 7.45 (d, J = 8.8 Hz, 2H), 7.39 (d, J = 16.4 Hz, 1H), 7.33 (s, 2H, D_2O exchangable), 7.08 (d, J = 16.4 Hz, 1H), 6.67 (d, J = 8.8 Hz, 2H), 6.37 (d, J = 1.6 Hz, 1H), 5.43 (dd, 1H, J = 1.9, 6.1 Hz, 1H), 5.40 (dd, 1H, J = 1.6, 6.1 Hz, 1H), 4.57 (d, J = 1.9 Hz, 1H), 3.31-3.24 (m, 6H), 1.54 (s, 3H), 1.34 (s, 3H), 1.03 (t, J = 7.0 Hz, 3H). ^{13}C NMR (63 MHz, DMSO-d_6): δ 168.9 (C), 156.0 (C), 152.4 (CH), 148.8 (C), 148.1 (C), 145.3 (C), 145.1 (C), 140.5 (CH), 133.9 (CH), 128.7 (CH), 126.2 (CH), 124.0 (CH), 123.4 (C), 120.7 (CH), 118.9 (C), 112.9 (C), 111.3 (CH), 89.5 (CH), 86.0 (CH), 83.2 (CH), 83.1 (CH), 47.7 (CH_2), 44.2 (CH_2), 35.7 (CH_2), 26.7 (CH_3), 25.0 (CH_3), 12.0 (CH_3). MS: m/z = 615 (MH^+). Anal. calcd for $C_{31}H_{34}N_8O_6$ (614.26), C 60.58, H 5.58, N 18.23. Found C 59.98, H 5.53, N 18.11.

*Compound **8***: HCl (1M, 20 mL) was added to a solution of **7** (0.75 g, 1.2 mmol) in THF (30 mL). After 24 h at 60 °C, saturated K_2CO_3 was added (pH ~ 10) and THF was evaporated. The precipitate was filtered, washed (pH ~ 7) and dried to afford **8** as a red solid (0.67 g, 96 %). ^{1}H NMR (250 MHz, DMSO-d_6): δ 9.16 (bt, 1H, D_2O exchangeable), 8.37 (s, 1H), 8.18 (d, J = 8.9 Hz, 2H), 8.08 (s, 1H), 7.76 (d, J = 8.9 Hz, 2H), 7.48 (d, J = 8.5 Hz, 2H), 7.41 (d, J = 16.3 Hz, 2H), 7.09 (d, J = 16.3 Hz, 2H), 6.78 (d, J = 8.5 Hz, 2H), 5.97 (d, J = 7.3 Hz, 1H), 5.78 (d, J = 4.3 Hz, 1H, D_2O exchangeable), 5.57 (d, J = 6.2 Hz, 1H, D_2O exchangeable), 4.62 (m, 1H), 4.33 (bs, 1H), 4.17 (dd, J = 4.3, 3.5 Hz, 1H), 3.42 (m, 6H), 1.08 (t, J = 6.9 Hz, 3H). ^{13}C NMR (125 MHz, DMSO-d_6): 170.0 (C), 161.8 (C), 156.2 (C), 152.6 (CH), 149.0 (C), 148.2 (C), 145.4 (C), 145.3 (C), 140.8 (CH), 134.1 (CH), 128.9 (CH), 126.4 (CH), 124.2 (C), 123.6 (CH), 120.9 (CH), 111.6 (CH), 87.9 (CH), 84.7 (CH), 73.0 (CH), 71.9 (CH),

48.7 (CH_2), 44.6 (CH_2), 36.5 (CH_2), 12.1 (CH_3). HRMS (ESI) calcd for $C_{28}H_{31}N_8O_6$ (MH^+) *m/z* 575.2367, found 575.2386.

*Compounds **9** and **10***: *n*Bu_2SnO (52 mg, 0.21 mmol) was added to a suspension of **8** (93 mg, 0.16 mmol) in anhydrous toluene (10 mL). After 2 h at 130°C under an Ar atmosphere, toluene was evaporated. Anhydrous CH_2Cl_2 (10 mL) and $ClP(O)(OEt)_2$ (47 μL, 0.32 mmol) were added to the reaction. After 48 h at RT, CH_2Cl_2 was evaporated off. THF (3 mL) and HCl (37%, 1.5 mL) were added and the mixture was stirred at RT for 2.5 h (TLC monitoring: 30:65:4:1 $CH_3OH–CH_2Cl_2–H_2O–Et_3N$). After addition of an aq. NH_3 solution (2%, until pH ~ 7), the deep-red solid was filtered, washed with H_2O. The crude product was dissolved in DMF and purified by chromatography over C_{18} silica gel (25:75:1 $CH_3CN–H_2O–2\%$ NH_4OH) to provide a mixture of the two regioisomers **9** and **10** in a ratio of 40:60 after lyophilization (76 mg, 70% from diol **8**).

*Compound **9*** (2'-PO_4H_2, 40 %): ^{1}H NMR (500 MHz, DMSO-d_6): δ 9.16 (bt, 1H), 8.40 (s, 1H), 8.17 (d, 2H, J = 8.9 Hz), 8.02 (s, 1H), 7.76 (d, 2H, J = 8.9 Hz), 7.48 (d, 2H, J = 9.1 Hz), 7.40 (m, 3H), 7.10 (d, 2H, J = 16.4 Hz), 6.78 (d, 2H, J = 9.1 Hz), 6.07 (d, 1H, J = 7.1 Hz), 4.83 (m, 1H), 4.49 (d, 1H, J = 3.8 Hz), 4.45 (bs, 1H), 3.44-3.35 (m, 6H), 1.09 (t, 3H, J = 7.0 Hz).
*Compound **10*** (3'-PO_4H_2, 60 %): ^{1}H NMR (500 MHz, DMSO-d_6): δ 9.26 (bt, 1H), 8.40 (s, 1H), 8.17 (d, 2H, J = 8.9 Hz), 8.02 (s, 1H), 7.76 (d, 2H, J = 8.9 Hz), 7.48 (d, 2H, J = 9.1 Hz), 7.40 (m, 3H), 7.10 (d, 2H, J = 16.4 Hz), 6.78 (d, 2H, J = 9.1 Hz), 5.97 (d, 1H, J = 8.2 Hz), 4.62 (m, 1H), 4.71 (m, 1H), 4.36 (bs, 1H), 3.44-3.35 (m, 6H), 1.09 (t, 3H, J = 7.0 Hz).

^{13}C NMR (125 MHz, DMSO-d_6): δ 169.9 (C), 169.5 (C), 156.2 (C), 152.4 (CH), 148.9 (C), 148.0 (C), 145.3 (C), 145.0 (C), 140.5 (CH), 134.0 (CH), 128.8 (CH), 126.2 (CH), 124.0 (CH), 123.4 (C), 120.8 (CH), 111.4 (CH), 88.3 (CH), 83.9 + 83.6 (CH), 75.7 (CH), 72.3 (CH), 48.7 + 48.6 (CH_2), 44.8 + 44.5 (CH_2), 36.4 (CH_2), 12.0 (CH_3).

HRMS (ESI^-) calcd for $C_{28}H_{30}N_8O_9P$ $[M-H]^-$653.1873, found 653.1877.

Biochemistry, General. L-Arginine, (6R)-5,6,7,8-tetrahydrobiopterin (H_4B), calmodulin (CaM), Hepes, Tris-HCl, $CaCl_2$, NADPH, glycerol, cytochrome *c* (cyt *c*), myoglobin, ferredoxin reductase ($ferredoxin_{red}$) and ferredoxin (from spinach), isocitrate dehydrogenase, glucose 6-phosphate dehydrogenase were purchased from Sigma-Aldrich.

***Expression and purification of proteins*.** Recombinant full-length rat nNOS, murine iNOS and bovine eNOS were expressed in *Escherichia coli* cell line BL21 (DE3) and purified as previously described (14-17). The heme content was determined optically from the [CO-reduced]-[reduced] difference spectrum using $\Delta\varepsilon_{444\text{-}470\ nm}$ = 76,000 M^{-1} cm^{-1} (18). Recombinant reductase domain of eNOS ($eNOS_{red}$) was overexpressed in yeast and purified as described (15, 19). Purified nNOS, eNOS, iNOS and $eNOS_{red}$ were more than 95 % pure as determined by SDS–PAGE stained with Coomassie Blue. Fatty acid binding protein (FABP) was a generous gift of Dr Jiayao Li (LBPA). Cytochrome P450 reductase ($P450_{red}$) was a gift of Dr Lee-Ho Wang (UTHSC, TX, USA). Lens epithelium-derived growth factor (LEDGF) and *E. Coli* RecQ helicase were prepared as reported in (20, 21). Protein contents were measured using the Bradford reagent from BioRad and bovine serum albumin as a standard.

***Spectroscopic methods: Characterization of free or NOS-bound NS1*.** UV-visible absorption spectrum of NS1 was carried out with an Uvikon XL spectrophotometer. NS1-binding isotherms were build using NOS in 50 mM Tris pH 7.5 containing 150 mM NaCl at 25 °C, either under one-photon (1-PE) or two-photon excitation (2-PE) conditions. For one-photon experiments, fluorescence excitation and emission spectra were recorded on a Eclipse (Varian) spectrofluorimeter, equipped with a thermostated cell holder, using aerated 80 µl solutions placed in micro cells (Hellma, Paris, France). The emission spectra were recorded with excitation and emission slits set at 5 nm. Two-photon excitation and emission spectra were recorded using a home-built set-up. Briefly, a 80-MHz mode-locked Mai-Tai® Ti:Sapphire tunable laser (690-1040 nm, 100 fs laser pulse; Spectra Physics, Mountain View, CA, USA) was focused onto the sample (80 µl) placed in a quartz micro cell. The two-photon fluorescence was collected at 90 degrees and was further filtered by a Semrock FF01-842/SP filter to reject the residual excitation light. The fluorescence signal was focused into an optical fiber connected to a SpectraPro-275 digital spectrograph (300 lines/mm) coupled to a liquid nitrogen cooled CCD detector (1024 × 256 pixels; Princeton Instruments Acton, MA, USA). The wavelength calibration of the spectrograph was done using a high pressure mercury lamp. Excitation power was set between 50 and 100 mW and the acquisition time varied between 1 and 60 s.

Stopped-flow experiments. Kinetics of the reaction between nNOS and NADPH were measured at 24 °C in an anaerobic chamber (Coy Laboratory Products Inc., Michigan, USA), using a Bio-SEQUENTIAL DX-18MV stopped-flow instrument (Applied Photophysics, Leatherhead, UK). Measurements were carried out using an anaerobic solution of 5 µM nNOS (in 50 mM Hepes buffer, pH 7.7 containing 0.1 M NaCl, 10% glycerol, 1 mM L-arginine, 1 mM calcium and 25 µM CaM) and monitored at different wavelengths. The solutions of 25 µM NADPH and NS1 (0-100 µM) were prepared in oxygen-free buffer (50 mM Hepes, 0.1 M NaCl, 10 glycerol, pH 7.7). Kinetic rates were calculated by fitting data to a single or double-exponential functions using Applied Photophysics software.

Effect of NS1 on the formation of NO catalysed by nNOS. The initial rates of NO formation were determined at 37 °C in 1-cm path-length cuvettes (total volume of 150 µl) using the oxyhemoglobin assay for NO (22). Usual incubation mixtures were performed in 50 mM Hepes buffer (pH 7.4) containing, 0.1 M KCl, 5 mM DTT, 10-20 µM oxyhemoglobin, 100 U/ml each of SOD and catalase, 10 µM H_4B, 100 µM L-arginine, 1 mM $CaCl_2$, 10 µg/ml CaM, 4-6 µg/ml nNOS, and 0-100 µM NS1. The mixtures were preincubated for 2 min at 37 °C prior to initiation of the reactions by the addition of NADPH (10-100 µM) to both cuvettes. The NO-mediated conversion of oxyhemoglobin to methemoglobin was monitored by repetitive scanning between 380 and 480 nm every 0.2 min on a Uvikon 941 spectrophotometer and quantified using an extinction coefficient of 77,000 $M^{-1}.cm^{-1}$ between peak at 401 nm and valley at 420 nm. Control incubations were performed in the presence of similar amounts of buffer without inhibitor. All values are expressed relative to the control and are means $\pm$ S.D. from 3-4 experiments.

Imaging of living HUVEC cells in the presence of NS1 and co-localization experiments. HUVECs (human umbilical vein endothelial cells, purchased from Sigma) were prepared as previously described (23). NS1 (final concentration, 5 µM) was incubated with HUVECs (at the fourth passage) for 30 min and the medium was changed before observation. One-photon images of living HUVECs were obtained using a SP2 confocal microscope (Leica MicroSystems, France) equipped with an incubation chamber (37°C, CO_2 5%). A laser line at 488 nm was used for the excitation of NS1 and the emission range was set between 520 and 680 nm. A similar set up was used for two-photon images except that the excitation source was a 80-MHz mode-locked Mai-Tai® Ti:Sapphire tunable laser (720-920 nm, 100 fs laser pulse; Spectra Physics, Mountain View, CA, USA) tuned to 840 nm. The image of nucleus was monitored using Hoechst 33342 using two-photon excitation (740 nm; emission setting: 410-510 nm).

Co-localization experiments of NS1 with endoplasmic reticulum (ER), mitochondria or Golgi complex were performed on living HUVEC cells (4-7th passage). ER-TrackerTM Red dye (Ref. no. E34250) for ER labeling, MitoTracker® Deep Red FM (Ref. no. M22426) for mitochondria labeling or BODIPY® TR Ceramide complexed to BSA (Ref. no. B34400) for Golgi complex labeling were purchased from Invitrogen (France).

Co-localization of NS1 with early endosome (EEA1) or eNOS was performed by immuno-staining on fixed HUVEC cells according to standard procedure (23, 24) with modifications: PBS-0.5% Saponin was used as permeabilization solution for 10 min at room temperature instead of PBS-0.2% Triton X-100 / 2 mg/ml BSA /1 mM NaN_3 on ice. Blocking solution was PBS-3% BSA instead of PBS / 0.02% Triton X-100 / 3% BSA /1 mM NaN_3. Purified mouse anti-eNOS/NOS Type III (BD-Biosciences, France); ref. no. 610297) and rabbit polyclonal to EEA1-Early Endosome Marker (abcam®, Cambridge, UK; ref. no. ab2900) primary antibodies were used at final concentrations of 10 and 4 µg/mL, respectively, in PBS-0.5% Saponin / 3% BSA. Secondary antibodies, AlexaFluor® 594 goat anti-mouse IgG (H+L) (Ref. no. A-11005) and AlexaFluor® 594 donkey anti-rabbit IgG (H+L) (Ref. no. A-11012) were purchased from Invitrogen (France) and used at final concentrations of 4 and 2 µg/mL, respectively, in PBS-0.5% Saponin / 3% BSA. The fixation buffer BD Cytofix™ was purchased from BD-Biosciences. Saponin from Quillaja bark and BSA were purchased from Sigma life science. The mounting medium CITIFLUOR™PERMAFIX 1 (HRF) was purchased from Biovalley (France). Excitation and emission settings are indicated in figure legends.

SUPPLEMENTARY REFERENCES:

1. Oivanen ML, H. (1989) Kinetics and mechanisms for reactions of adenosine 2'- and 3'-monophosphates in aqueous acid: competition between phosphate migration, dephosphorylation, and depurination. *J. Org. Chem.* 54:2556–2560.
2. Lambry JC, Beaumont E, Tarus B, Blanchard-Desce M, & Slama-Schwok A (2010) Selective probing of a NADPH site controlled light-induced enzymatic catalysis. *J Mol Recognit* 23:379-388.
3. Garcin ED, *et al.* (2004) Structural basis for isozyme-specific regulation of electron transfer in nitric-oxide synthase. *J Biol Chem* 279:37918-37927.
4. Panda SP, *et al.* (2006) The role of a conserved serine residue within hydrogen bonding distance of FAD in redox properties and the modulation of catalysis by Ca2+/calmodulin of constitutive nitric-oxide synthases. *J Biol Chem* 281:34246-34257.
5. Zhang J, Martasek, P, Paschke, R., Shea,T., SilverMasters, B.S., Kim, JJ (2001) Crystal structure of the FAD/NADPH-binding domain of rat neuronal nitric-oxide synthase. Comparisons with NADPH-cytochrome P450 oxidoreductase. *J. Biol. Chem.* 276:37506-37513.
6. Lapouyade R, Kuhn, A., Letard, J.F., Rettig, W. (1993) Multiple relaxation pathways in photoexcited dimethylaminonitro- and dimethylaminocyano-stilbenes. *Chem Phys. Lett.* 208:48-58.
7. Phillips JC, *et al.* (2005) Scalable molecular dynamics with NAMD. *J Comput Chem* 26:1781-1802.
8. Folloppe N, MacKerell, A.D. (2000) All-atom empirical force field for nucleic acids: I. Parameter optimization based on small molecule and condensed phase macromolecular target data. *J. Comp. Chem* 21:86-104.
9. Jorgensen WL, Chandrasekhar J, Madura JD, Impey RW, & Klein ML (1983) Comparison of simple potential functions for simulating liquid water. *J. Chem. Physiol.* 79:926-935.
10. Darden T, York DM, & Pedersen L (1993) Particle mesh Ewald: An N×log(N) method for Ewald sums in large systems. . *J. Chem. Phys.* 98:10089-10092.
11. Ryckaert JP, Ciccotti G, & Berendsen HJC (1977) Numerical-integration of Cartesian equations of motion of a system with constraints: Molecular dynamics of n-alkanes. *J. Comp. Phys.* 23:327-341.
12. Safavy A, Smith DC, Jr., Bazooband A, & Buchsbaum DJ (2002) De novo synthesis of a new diethylenetriaminepentaacetic acid (DTPA) bifunctional chelating agent. *Bioconjug Chem* 13(2):317-326.
13. Ha SB, Nair, V. (1996) An Improved Approach to the Synthesis of Adenosine-5'-N-Ethyluronamides of Interest as Adenosine Receptor Agonists *Tetrahedron letters* 37:1567-1570.
14. Berka V, Wang LH, & Tsai AL (2008) Oxygen-induced radical intermediates in the nNOS oxygenase domain regulated by L-arginine, tetrahydrobiopterin, and thiol. *Biochemistry* 47:405-420.
15. Du M, Yeh HC, Berka V, Wang LH, & Tsai AL (2003) Redox properties of human endothelial nitric-oxide synthase oxygenase and reductase domains purified from yeast expression system. *J Biol Chem* 278:6002-6011.
16. Moali C, Boucher JL, Sari MA, Stuehr DJ, & Mansuy D (1998) Substrate specificity of NO synthases: detailed comparison of L-arginine, homo-L-arginine, their N omega-hydroxy derivatives, and N omega-hydroxynor-L-arginine. *Biochemistry* 37:10453-10460.

17. Wu C, Zhang J, Abu-Soud H, Ghosh DK, & Stuehr DJ (1996) High-level expression of mouse inducible nitric oxide synthase in Escherichia coli requires coexpression with calmodulin. *Biochem Biophys Res Commun* 222:439-444.
18. Stuehr DJ & Ikeda-Saito M (1992) Spectral characterization of brain and macrophage nitric oxide synthases. Cytochrome P-450-like hemeproteins that contain a flavin semiquinone radical. *J Biol Chem* 267:20547-20550.
19. Raman CS, *et al.* (1998) Crystal structure of constitutive endothelial nitric oxide synthase: a paradigm for pterin function involving a novel metal center. *Cell* 95:939-950.
20. Li N, *et al.* (2010) Multiple Escherichia coli RecQ helicase monomers cooperate to unwind long DNA substrates: a fluorescence cross-correlation spectroscopy study. *J Biol Chem* 285:6922-6936.
21. Cherepanov P, *et al.* (2003) HIV-1 integrase forms stable tetramers and associates with LEDGF/p75 protein in human cells. *J Biol Chem* 278:372-381.
22. Murphy ME & Noack E (1994) Nitric oxide assay using hemoglobin method. *Methods Enzymol* 233:240-250.
23. Martinive P, *et al.* (2009) Impact of cyclic hypoxia on HIF-1alpha regulation in endothelial cells--new insights for anti-tumor treatments. *FEBS J* 276:509-518.
24. Kodiha MR, L.; Stochaj, U. (2009) Optimized immunofluorescence staining protocols to detect the nucleoporin Nup98 in different subcellular compartments. *Nature Protocol- Protocol Exchange*:doi:10.1038/protex.2010.1211